Catalysis Today xxx (2016) xxx–xxx

Contents lists available at ScienceDirect

Catalysis Today

journal homepage: www.elsevier.com/locate/cattod

Ni-based structured catalyst for selective 3-phase hydrogenation of nitroaromatics

Oliver Beswick[a], Daniel Lamey[a], Félicien Muriset[a], Thomas LaGrange[b], Loïc Oberson[b], Songhak Yoon[c], Esther Sulman[d], Paul J. Dyson[a], Lioubov Kiwi-Minsker[a,d,*]

[a] Group of Catalytic Reaction Engineering, Ecole Polytechnique Fédérale de Lausanne (EPFL), Station 6, Lausanne CH-1015, Switzerland
[b] Interdisciplinary Centre for Electron Microscopy (CIME), Ecole Polytechnique Fédérale de Lausanne (EPFL), Station 12, Lausanne CH-1015, Switzerland
[c] Laboratory for Solid State Chemistry and Catalysis, Swiss Federal Laboratories for Materials Science and Technology (EMPA), 8600 Dübendorf, Switzerland
[d] Regional Technological Centre, Tver State University, 170100 Tver, Russian Federation

ARTICLE INFO

Article history:
Received 1 December 2015
Received in revised form 19 April 2016
Accepted 25 April 2016
Available online xxx

Keywords:
Selective hydrogenation
Nitrobenzene
p-Chloroaniline
Ni nanoparticles
Activated carbon fibres
Structured catalyst

ABSTRACT

We report herein on the development of Ni-based catalyst using activated carbon fibres (ACFs) as a structured support and its application for the three-phase hydrogenation of nitroarenes ($T = 353$ K; $P = 10$ bar). It was shown that metallic Ni^0 nanoparticles (NPs) with a mean diameter of ~2.0 nm stabilized by the ACF microporous network were responsible for the catalytic transformation. To obtain optimum catalytic activity, the Ni/ACF catalyst must be freshly prepared and activated *in situ* by H_2 at T > 353 K. Pre-treatment of the ACFs by nitric acid boosted the activity of the Ni/ACF catalyst, which exhibits high performance in hydrogenation of nitrobenzene to aniline (yield, Y ~100%). The catalyst was tested for the reuse attaining a quasi-steady-state after the sixth reaction thereafter remaining relatively stable over seven consecutive runs. Near-quantitative transformation (Y > 99%) of *p*-chloronitrobenzene to *p*-chloroaniline was achieved under mild conditions over the Ni/ACF catalyst with a *ca.* 20-fold higher activity than conventional Raney Ni. Thus, new catalyst reported here represents a significant step forward towards a simple, heterogeneous catalytic selective hydrogenation of nitroarenes that employs H_2 as the hydrogen source.

1. Introduction

Functionalized anilines are valuable intermediates used in the synthesis of agrochemicals, pharmaceuticals, pigments and dyes [1]. They are generally prepared by hydrogenation of the corresponding nitroarenes. Traditional non-catalytic processes have been largely abandoned, being replaced by catalytic hydrogenation processes [2]. The catalytic route allows high yields without the generation of toxic wastes and smaller amount of by-products with cost efficient separation and treatment processes. For substituted anilines the preservation of functional groups is one of the main challenges, with the exclusive reduction of the nitro-group while not affecting other groups being crucial [1,3].

The majority of heterogeneous catalytic systems used to hydrogenate nitroarenes are based on precious metals such as Au, Pd, Pt, Rh or Ru [4–14]. Nevertheless, catalysts based on Fe, Co, Cu or Ni [1,9,11,15–19] show promising activity in both liquid and gas-phases [1,18] while Raney nickel is the only commercial catalyst used on the industrial scale for Cl-nitroarenes hydrogenation [1]. The influence of metal nanoparticles (NPs) size on catalytic response including the catalyst selectivity and stability has been widely reported [20–25], although the control of the NP size during the preparation of supported catalysts is difficult to ensure. In general, the highest dispersion of active metal is targeted in order to have a sufficient catalytic performance per mole of active metal.

The majority of hydrogenation catalysts are used as powders to avoid transport limitations, but these powders lead to problems during downstream separation. Possible solutions lie in the use of structured catalysts that allow simple handling and controlled fluid dynamics [14,26]. ACFs in the form of tissues are ideal catalytic structured supports, characterized by a highly porous network, high specific surface areas (SSAs) (up to 3000 $m^2\ g^{-1}$) and low resistance to fluid flow [10,27–30]. ACFs have been used for the deposition of noble metal NPs and exhibit good performances in the multi-phase hydrogenation [31–34]. The carbonaceous surface can be pre-treated in acidic media generating different oxygen-containing groups [35,36]. In this way, the morphology of the supported Me NPs and their catalytic response can be controlled.

* Corresponding author at: Group of Catalytic Reaction Engineering, Ecole Polytechnique Fédérale de Lausanne (EPFL), Station 6, Lausanne CH-1015, Switzerland.
E-mail address: lioubov.kiwi-minsker@epfl.ch (L. Kiwi-Minsker).

http://dx.doi.org/10.1016/j.cattod.2016.04.020
0920-5861/

Herein, we present a facile preparation of ACF-based structured catalysts with supported Ni-NPs of high dispersion (1–2 nm) as an active phase. Different pre-treatments of ACF were applied and the influence of preparation conditions on catalytic response has been assessed in nitroarenes hydrogenation. A battery of physico-chemical techniques, such as N_2 physisorption, XRD, XPS, AAS, SEM, STEM-HAADF imaging, temperature programmed decomposition (TPD) and reduction by hydrogen (TPR) was applied for catalysts characterization. The activity/selectivity of the various Ni/ACF catalysts was compared to industrial Raney nickel which serves as a benchmark catalyst.

2. Experimental

2.1. Materials

Nickel(II) nitrate hexahydrate (Fluka, ≥98.0%), nitric acid (VWR chemicals, 65%), hydrogen peroxide (reactolab SA, 30%), nitrobenzene (99%, Acros Organics), 1-chloro-4-nitrobenzene (99%, Acros Organics), 1,3-dinitrobenzene (Tokyo Chemical Industry, ≥99.0%), dodecane (99%, Acros Organics), methanol (MeOH, ≥99.8%, Sigma-Aldrich), ethanol (EtOH, 99.8%, Sigma-Aldrich), toluene (>99%, AppliChem) were used as received. The solvent used for the reaction was technical EtOH (95% + 5% MeOH, Brenntag). All gases (H_2, N_2, and Ar) were of high purity (Carbagas Switzerland, >99.9%). The ACF K-20 (~2000 $m^2\ g^{-1}$) was purchased from Kynol Europa GmbH.

2.2. Catalyst preparation

2.2.1. Structured Ni/ACF

The Ni/ACF catalysts were prepared as follows. Commercial ACF was pre-treated in 15 wt.% HNO_3 aq. solution for 15 min at 373 K ($ACF_{HNO3\text{-}373}$) and for 3 min at 298 K ($ACF_{HNO3\text{-}298}$) to increase the concentration of oxygen-containing groups on the carbon surface [35,37]. The supports denoted as ACF were not pre-treated and used as received. The ACF was impregnated with an ethanolic solution of the Ni precursor ($Ni(NO_3)_2{\cdot}6H_2O$) ensuring complete filling of the pores. The Ni loading was adjusted by varying the precursor concentration. The impregnated ACF samples were dried at room temperature (RT) overnight. The precursor decomposition was performed *via* thermal treatment in a flow reactor (50 cm × 3 cm i.d.) from RT to 673 K, 6 K min^{-1} under Ar flow (280 $cm^3\ min^{-1}$), maintained at 673 K (1 h) under 17% v/v H_2/Ar flow (340 $cm^3\ min^{-1}$) and cooled to RT under Ar. To prevent oxidation of the pyrophoric Ni/ACF, the samples were passivated (1 h) at RT in 2.8% v/v air/Ar flow (145 $cm^3\ min^{-1}$). Gas flows were controlled using an *Agilent Technologies* ADM1000 Universal Gas Flowmeter, values are given in IUPAC STP [40].

2.2.2. Raney nickel catalyst

1 g of Ni-Al (50:50 wt.% alloy, Alfa Aesar) was treated with an aq. solution of KOH (10 wt.%) and stirred at RT until bubbling (H_2) stopped (~1 h), then at 333 K for 0.5 h. The resulting solid (Raney Ni) was decanted, washed with distilled water and ethanol.

2.3. Catalyst characterization

The Ni content was determined by absorption atomic spectroscopy (AAS) using a Shimadzu AA-6650 spectrometer with an air-acetylene flame. Temperature-programmed reduction in hydrogen (H_2-TPR) was carried out on a Micromeritics Autochem II 2920 by heating the sample in 17 $cm^3\ min^{-1}$ 5% v/v H_2/N_2 from RT to 973 K at 2 K min^{-1}. The exit gas was passed through a liquid N_2 trap and changes in H_2 consumption/release were monitored by TCD with data acquisition/manipulation using the TPR Win™ software.

BET surface areas were measured using a Micromeritics 3Flex. Prior to analysis, the samples were degassed at 393 K for 3 h under vacuum ($<1 \times 10^{-5}$ bar). N_2 adsorption/desorption isotherms were recorded over the range $0.000002 \leq P/P_0 \leq 0.99$. The specific surface area and the total pore volume were obtained using the BET method [38].

Temperature Programmed Decomposition (TPD) was conducted in a He flow (50 $cm^3\ min^{-1}$) from RT to 835 K at 5 K min^{-1} in a tubular reactor inside an oven (Carbolite MTF 10/25/130) and the outlet flow was continuously monitored using a Pfeiffer Vacuum ThermoStar™ GSD 300 T2. The NO_2 signal was mainly detected as a NO fragment ($m/z = 30$).

Powder X-ray diffractograms (XRD) were recorded on a Bruker/Siemens D500 incident X-ray diffractometer using Cu Kα radiation. The samples were scanned at 0.004° s^{-1} over the range $20° \leq 2\theta \leq 90°$ (scan time = 5 s $step^{-1}$). Diffractograms were identified using the JCPDS-ICDD reference standard, *i.e.* Ni (89-7129), NiO (89-5881) and NiO_2 (89-8397). *In situ* XRD patterns were obtained using a PANalytical X'Pert PRO θ–θ scan system with $Cu_{K\alpha}$ radiation (λ = 1.5418 Å). The diffraction patterns were recorded at a scanning rate of 0.015° s^{-1}. The $Ni(NO_3)_2/ACF_{HNO3\text{-}373}$ sample was placed in the heating chamber (XRK 900, Anton Paar) and gas was applied through the mass flow controller (5850 TR, Brooks instrument). About 0.03 g of sample was heated under a 60 $cm^3\ min^{-1}$ flow of N_2 up to 723 K with a heating rate of 2 K min^{-1}. Long scans ($30° \leq 2\theta \leq 85°$) were acquired on the fresh sample directly after heating to 723 K. In a separate experiment on the same starting material, the procedure was modified by replacing the N_2 by 10% v/v H_2/N_2. A long scan was performed at the end of the procedure. Peak fitting was performed using the *EVA (DIFFRAC.Suite)* software.

X-ray photoelectron spectroscopy (XPS) analysis was conducted on PHI VersaProbe II (Physical Instruments AG). The monochromatic Al Kα X-ray source power was maintained at 24.8 W and the emitted photoelectrons were obtained from a 100 μm × 100 μm samples. The spherical capacitor analyser was set at a 45° take-off angle with respect to the sample surface. The analyser pass energy was 188 eV for survey spectra (0–1300 eV) and 47 eV for high resolution spectra (Ni 2p3/2 and Ni 2p1/2). For the latter resolution a full width at half maximum of 0.91 eV for the Ag 3d 5/2 peak was obtained. The adventitious C (284.8 eV) 1 s peak was used as an internal standard to compensate for any charging effects. Sputtering was realized using a 20 kV Ar_{2500}^+ cluster source on a 2 nm × 2 nm sample surface at a rate of 0.45 nm/min (referenced to SiO_2). Curve fitting was performed using the CasaXPS software.

The Ni NPs size distribution was measured from "Z-contrast" or high angle annular dark-field scanning transmission electron microscope (HAADF STEM) images acquired on a FEI Talos F200S instrument operating at 200 keV. The Ni/ACF catalysts were infiltrated-embedded in an EPON 812 epoxy resin and polymerized at 333 K for 24 h, cut (20 nm) by ultramicrotomy to analyse the fibre cross-section. The TEM samples were subjected to mild (10 eV) plasma cleaning for 1 min using a Fischone 8070 plasma cleaner operated with a forward power of 9 W.

Up to 1400 individual metal particles were counted for the investigated catalyst and the circular diameter (d_i) was determined from the area measured using imageJ software from images of different magnifications. The mean circular diameter (d) was calculated using Eq. (1):

$$d = \frac{\sum_i n_i d_i}{\sum_i n_i} \quad (1)$$

where n_i is the number of particles of diameter d_i.

Please cite this article in press as: O. Beswick, et al., Ni-based structured catalyst for selective 3-phase hydrogenation of nitroaromatics, Catal. Today (2016), http://dx.doi.org/10.1016/j.cattod.2016.04.020

2.4. Hydrogenation of nitroaromatic compounds: set-up and analytics

Liquid phase hydrogenation reactions (T = 353–423 K; P_{H_2} = 10 bar) were carried out in a commercial semi-batch stirred reactor (150 cm^3 stainless steel autoclave, Büchi AG, Uster, Switzerland) equipped with baffles. The reactor temperature was controlled using a water heating bath (Colora K4, Lorch, Germany) connected to the reactor jacket. Mixing was achieved with a stirrer with a 6-blade disk turbine impeller and four wire-mesh blades onto which the structured ACF catalyst was fixed. The pressure and temperature inside the reactor as well as the stirring speed were monitored *via* a control unit (bpc 6002/bds mc, Büchi AG, Uster, Switzerland). Prior to each experiment, the reactor was charged with the catalyst and 100 cm^3 of an ethanolic solution of dodecane 1 g L^{-1} (internal standard) and flushed with N_2. The reactor was then heated to 353 K under stirring (2000 rpm) and stabilized for 5 min. H_2 was introduced into the reactor to a total pressure of 10 bar (sum of the partial pressures of EtOH and H_2), which was maintained throughout the reaction. The catalyst was reduced *in-situ* for 30 min. The substrate was subsequently injected (time t = 0) *via* a gas-tight syringe.

An initial NO_2/Ni molar ratio of 50 was targeted. A non-invasive liquid sampling system allowed the controlled removal of aliquots (≤0.4 cm^3) which were analysed using a Perkin-Elmer Clarus 500 GC equipped with programmed split/splitless injector, FID and Stabilwax (Cross-bond Carbowax-PEG, Restek, USA) capillary column (i.d. = 0.32 mm, length 30 m, film thickness 0.25 μm). Data acquisition/manipulations were performed using TotalChrom Workstation v.6.3.2. The concentrations of organic species and the conversion of the substrate, A, is defined using Eq. (2):

$$X_A(\%) = \frac{C_{A,0} - C_{A,i}}{C_{A,0}} \times 100 \quad (2)$$

where $C_{A,0}$ and $C_{A,i}$ represent the substrate molar concentrations at the beginning and time t, respectively. The selectivity towards product B is calculated using Eq. (3):

$$S_B(\%) = \frac{C_B}{C_{A,0} - C_{A,i}} \times \frac{\upsilon_A}{\upsilon_B} \times 100 \quad (3)$$

where C_{B0} and C_B represent the molar concentrations of product B at the beginning and time t, respectively, and ν_A and ν_B correspond to the stoichiometric coefficients.

The yield towards the product B with respect to substrate A is defined from Eq. (4):

$$Y_B(\%) = \frac{C_{B,0} - C_{B,i}}{C_{A,0}} \cdot \frac{\upsilon_A}{\upsilon_B} \times 100 \quad (4)$$

Repeated reaction runs with the same batch of the catalyst delivered values of the reaction mixture compositions that were reproducible to within ±4%. The catalytic activity was quantified in terms of the initial substrate consumption rate ($-R_{A,0}$) determined from a linear regression of the temporal substrate concentration profile, Eq. (5):

$$-R_{A,0}(\mathrm{mol_A mol_{Ni}^{-1} min^{-1}}) = \frac{(C_{A,0} - C_A) \cdot V}{n_{Ni} \cdot t_R} \quad (5)$$

where V is the reaction volume, n_{Ni} is the number of moles of Ni, and t_R the reaction time.

3. Results and discussion

3.1. Catalyst characterization

In order to rationalize the observed catalytic results, all samples were characterised by different physico-chemical methods.

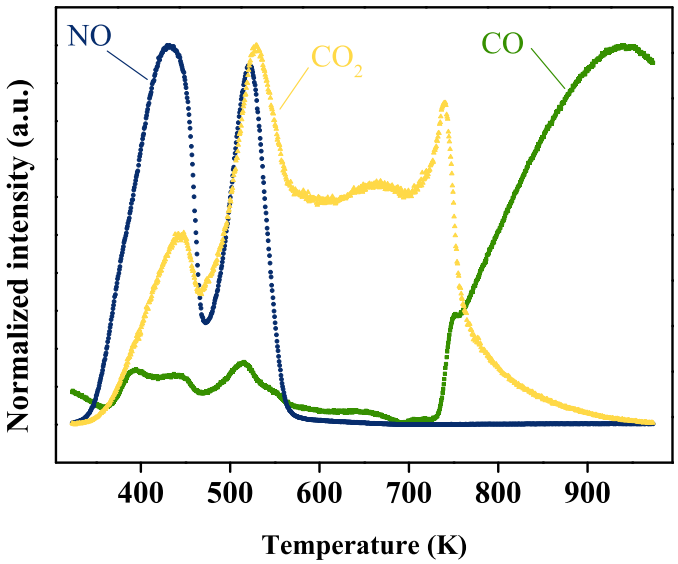

Fig. 1. TPD profile of $Ni(NO_3)_2/ACF_{HNO3\text{-}373}$ (■ CO; ▲ CO_2; ◆ NO).

3.1.1. BET

BET analyses were performed with different ACF samples and the associated SSAs and pore volumes are summarized in Table 1. A very high SSA (>2000 m^2 g^{-1}) was found for the as received, non-treated ACF (entry 1). Nitric acid treatment at 373 K decreased both the SSA and the pore volume. This effect has been already reported by Shim et al. [39] and is due to: *i)* the increased amount of functional O-groups on the surface and *ii)* a change in the carbon morphology. By heating under an inert gas the HNO_3 pre-treated ACF recovered the initial SSA and the total pore volume. It is plausible that the O-containing groups rendered part of the porous structure inaccessible for nitrogen adsorption. The deposition of 5 wt.% Ni (entries 4 and 5) changed only slightly the SSA (by 5–8%) and the pore volume of the ACF compared to the initial value, indicating that the deposition of the metal salt does not lead to pore blocking [40].

3.1.2. Temperature programmed decomposition (TPD) and reduction (TPR)

The ACF freshly impregnated by the Ni precursor, after drying, was studied by TPD to determine the decomposition of the precursor. The NO signal at the reactor outlet was monitored and the results are presented in Fig. 1. The NO peak at 432 K corresponds to the decomposition (323–473 K) of the surface nitrates leading to the formation of NO_2 [41]. The second NO peak at 521 K results exclusively from the decomposition of the HNO_3 vapour (473 K–573 K) into NO_2 [42]. At the end of the calcination step NiO NPs are formed. Therefore, during catalyst preparation, the calcination step was at 673 K to ensure complete decomposition of the nitrates. The surface O-groups are decomposed giving CO and CO_2 during TPD runs [37].

In order to choose a suitable reduction temperature, after the calcination step the catalyst was studied by TPR. The H_2-TPR profile of the $NiO_x/ACF_{HNO3\text{-}373}$ material exhibits two peaks at 602 and 778 K (Fig. 2A). The first one (602 K) is attributed to the reduction of NiO_x NPs and the second one is due to methanation of ACF. Performing the same procedure with MS instead of TCD confirmed the peak attribution to CH_4, H_2 and H_2O signals. Therefore, the reduction step during the catalyst preparation was set at 673 K for 1 h to ensure formation of metallic Ni NPs while minimizing detrimental methanation of the ACF support.

Catalytic testing has demonstrated that *in-situ* activation under H_2 of freshly prepared catalysts was necessary to obtain significant

Please cite this article in press as: O. Beswick, et al., Ni-based structured catalyst for selective 3-phase hydrogenation of nitroaromatics, Catal. Today (2016), http://dx.doi.org/10.1016/j.cattod.2016.04.020

Table 1
BET analysis for ACF support with and without acid treatment and Ni/ACF catalysts.

N°	Sample	Ni content (wt%)	Comment	SSA ± 50 ($m^2\ g^{-1}$)	Specific pore volume ± 0.02 ($cm^3\ g^{-1}$)
1	ACF	0	as received	2120	0.88
2	$ACF_{HNO3-373}$	0	HNO_3 treated[a]	1750	0.73
3	$ACF_{HNO3-373-\Delta}$	0	HNO_3[a] + thermal treatment in Ar at 673 K	2000	0.84
4	Ni/ACF	4.8	Calcination 673 K – reduction 673 K – passivation at RT	1960	0.83
5	$Ni/ACF_{HNO3-373}$	3.8	Calcination 673 K – reduction 673 K – passivation at RT	2000	0.79

[a] Treated with nitric acid: 15% HNO_3, 373 K, 15 min.

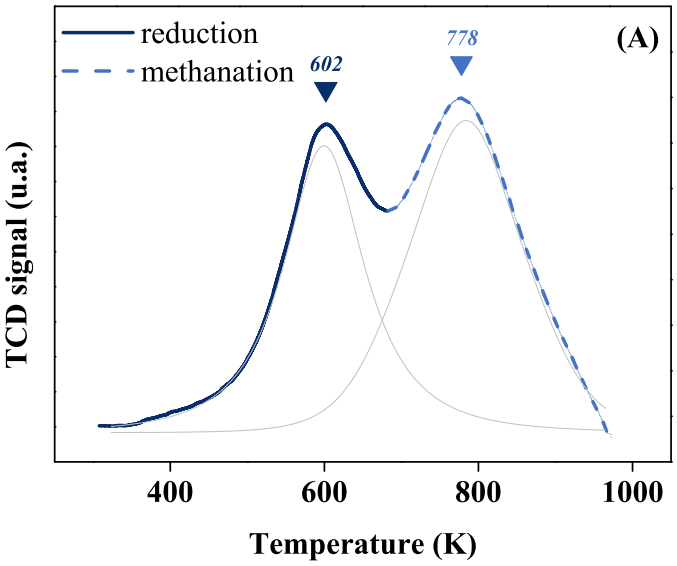

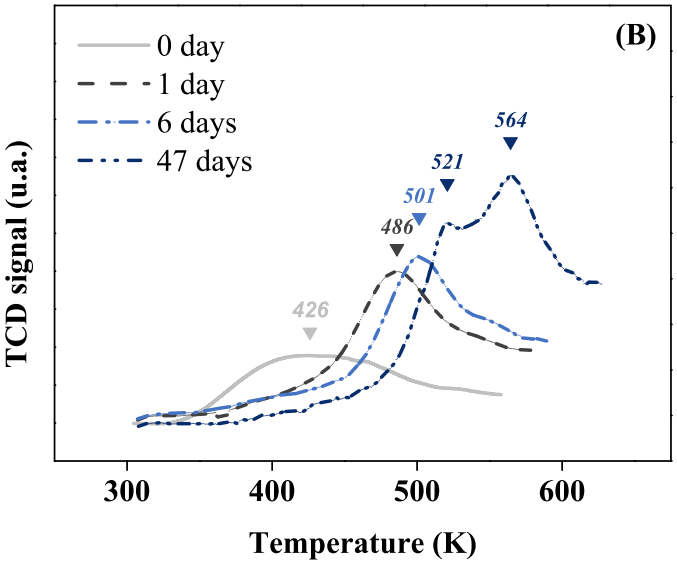

Fig. 2. TPR-H_2 profile of (A) $NiO_x/ACF_{HNO3-373}$ (after nitrates decomposition) and (B) $Ni/ACF_{HNO3-373}$ after reduction, passivation and exposition in air during different time.

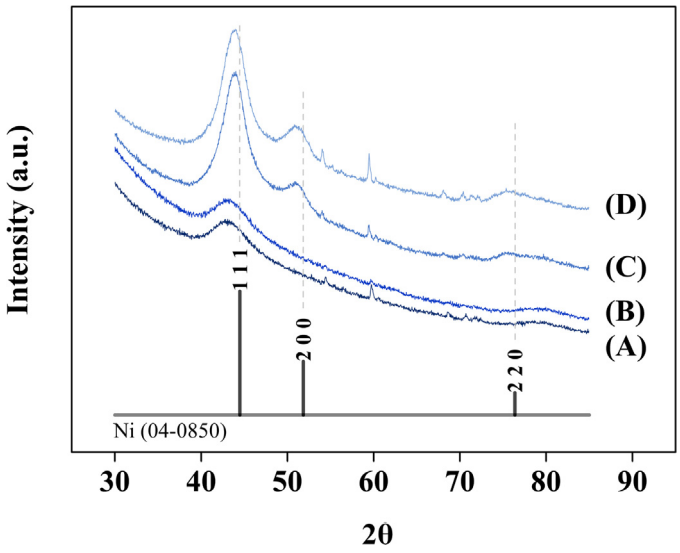

Fig. 3. *In-situ* XRD profile of ACF (A), $Ni(NO_3)_2/ACF_{HNO3-373}$ before (B) and after treatments in N_2 (C) and N_2/H_2 (D) at 723 K with JCPDS-ICDD reference diffractogram for Ni^0 (standard card 04-0850).

catalytic activity. Since the catalyst was passivated after reduction, this activation seems to be responsible for the removal of thin oxide layer from the Ni NPs surface. To confirm this assumption and to get a better insight on the dynamics of oxidation of the Ni NPs, the passivated samples were exposed to air for different periods of time and analysed by H_2-TPR. Without exposure to air (0 day, Fig. 2B) the hydrogen consumption was lower with the maximum at 426 K. Therefore, the Ni-oxides species are readily reducible during *in-situ* activation. The longer was the air exposure time, the higher the temperature and the larger the hydrogen consumption. The H_2-TPR profile of the sample exposed for to air 24 h exhibited a peak maximum at 486 K and for the sample exposed for 6 days a peak maximum was at 501 K. After 47 days of air exposure the profile has two peaks at 521 and 564 K, suggesting that to activate the catalyst *in-situ* a temperature of 353 K is not enough.

3.1.3. In-situ *XRD analysis*

The nature of the Ni phase was studied *in-situ* by XRD analysis following each step of the precursor decomposition/reduction until no more changes were observed to the diffraction pattern. Pattern A shown in Fig. 3 represents the initial ACF support and pattern B corresponds to the ACF after deposition of the $Ni(NO_3)_2{\cdot}6H_2O$ precursor. A sample of impregnated ACF was subjected to a thermal treatment (298 K–723 K, 2 K min^{-1}) under a 60 $cm^3\ min^{-1}$ flow of N_2 and left during one hour at the final temperature (Fig. 3**C**). Finally, pattern D represents the impregnated sample subjected to a thermal treatment (298 K–723 K, 2 K min^{-1}) under a 60 $cm^3\ min^{-1}$ flow of 10% v/v H_2/N_2. Diffraction patterns C and D show additional components compared to patterns A and B, suggesting that both N_2 and H_2/N_2 treatments lead to the formation of a $Ni^{(0)}$ phase by comparison with the JCPDS-ICDD reference standard, *i.e.* fcc Ni (04-0850).

The XRD analysis of the passivated $Ni/ACF_{HNO3-373}$ catalyst exposed to air over 6 days generated the pattern shown in Fig. 4. The profile exhibits four main peaks over the 2θ range 20°–90°, corresponding to the (222), (400), (440) and (440) planes of face-centred cubic NiO (JCPDS-ICDD 89-5881), and confirming the presence of nickel oxide after the standard treatment and air exposure.

Please cite this article in press as: O. Beswick, et al., Ni-based structured catalyst for selective 3-phase hydrogenation of nitroaromatics, Catal. Today (2016), http://dx.doi.org/10.1016/j.cattod.2016.04.020

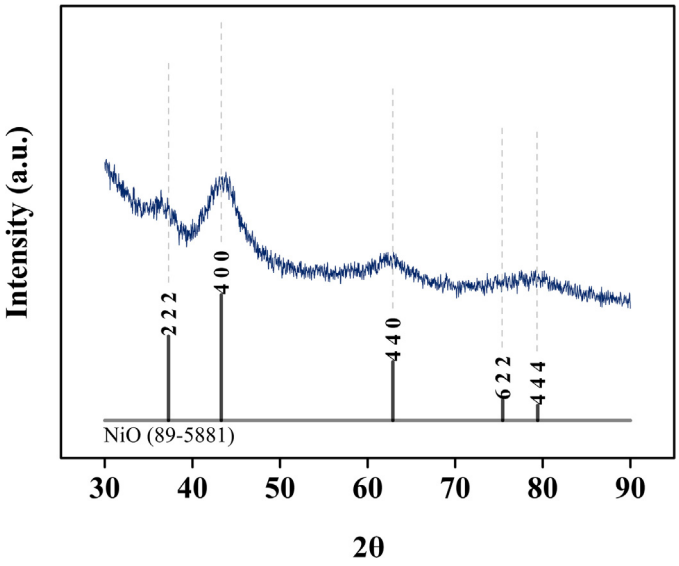

Fig. 4. XRD pattern of Ni/ACF$_{HNO3-373}$ after 6 days of exposure in air with JCPDS-ICDD reference diffractogram for NiO (standard card 89-5881).

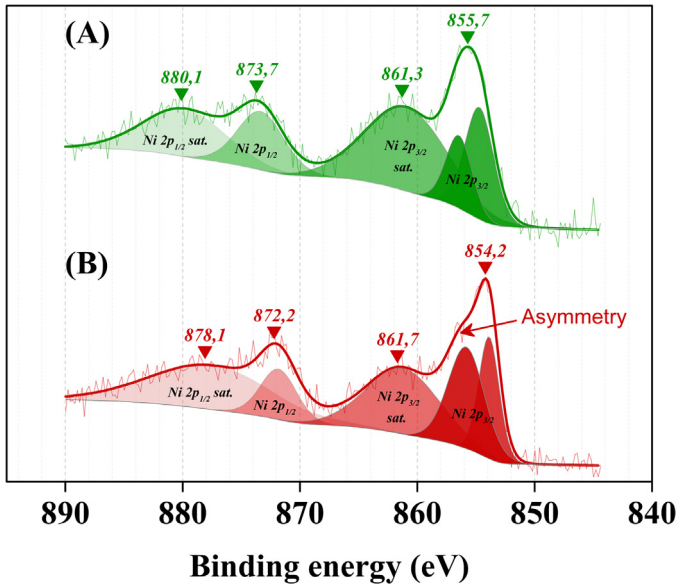

Fig. 5. XPS profiles of freshly prepared Ni/ACF$_{HNO3-373}$ (A) before and (B) after 5 min of Ar sputtering.

3.1.4. XPS analysis

Freshly prepared passivated Ni/ACF$_{HNO3-373}$ was studied by XPS before and after argon sputtering to gain information on the Ni NPs composition. Before sputtering the profile exhibits a symmetric Ni $2p_{3/2}$ peak at 855.7 eV and its satellite at 861.3 eV, respectively (Fig. 5A). The contributions of the main peak of NiO produce two visible maxima (at 853.7 and 855.4 eV) whereas a single symmetric peak is detected corresponding to $Ni(OH)_2$ [43]. The higher intensity of the Ni $2p_{1/2}$ peak measured at 873.7 eV compared to the satellite at 880.1, indicates that the NPs surface consists mainly of $Ni(OH)_2$. A contribution of NiO cannot be completely ruled out since the carbonaceous nature of catalyst results in low signal-to-signal.

After 5 min of Ar sputtering (2 nm) the position of the Ni $2p_{3/2}$ peak maxima was found to be shifted by 1.5 eV to 854.2 eV (Fig. 5B). The shape presents an asymmetry visible on the left side of the peak that is characteristic of a NiO contribution. The position of the Ni $2p_{1/2}$ peak satellite at 878.1 eV, half-way from NiO (879 eV) and Ni^0 (874 eV), could indicate some contributions from Ni^0.

In summary, XRD and XPS studies confirm that the conditions of Ni/ACF preparation lead to the formation of metallic Ni^0 NPs during the reduction under hydrogen. These particles were covered by a thin Ni-oxide/hydroxide layer formed during the passivation step.

3.1.5. STEM

HAADF STEM measurements were performed to observe the size and morphology of the Ni NPs. In the images they appear as bright contrast within the ACF support composed of a lower density carbon material (Z-contrast).

Fig. 6 shows the image of Ni/ACF$_{HNO3-373}$ (A) and outlines of the Ni NPs of the same sample (B). The STEM derived histogram for this sample (C) is characterized by a distribution of the NP size between 1.6–2.6 nm with 53% within the range. The mean particle diameter was found 2.1 ± 1 nm. Analysis of NiO_x/ACF (with non-treated by HNO_3 support) reveals NPs in the range of 1.4–2.3 nm for 52% of the NPs with a mean particle size of 1.7 ± 0.8 nm. The mean diameter of NiO_x NPs on acid pre-treated support, ACF$_{HNO3-373}$, formed before the reduction in H_2-flow (images not shown) is 1.8 ± 0.9 nm, being similar to those without acid treatment.

Thus, the thermal treatment in the presence of hydrogen leads to a slight increase of mean NPs size. Note that the presence of particles with sizes below the detection threshold, not visible with the high magnification (1.3 Mx), cannot be excluded. Imaging with the aberration corrected microscope (FEI Titan Themis) of the Ni/ACF$_{HNO3-373}$ specimen suggested that a larger proportion of NPs in the sub-nm range (0.5–1 nm) exist than detected with the FEI Talos F200S. The enhanced catalytic properties of these sub-nm range NPs could arise from their irregular shape and dangling chains of atoms on the surface, increasing the number active sites. Also, the distribution of the Ni/ACF$_{HNO3-373}$ specimen (Fig. 6C) suggests that the Ni-NPs are attached rather than stacked. Therefore, the effective NPs surface available for catalysis might be greater for this sample, despite its larger mean diameter.

In summary, the oxidative pre-treatment of ACF support by HNO_3 weakly affects the NiO_x NPs size. In contrast, the reductive treatment at 673 K slightly diminishes the Ni-NPs dispersion with a concomitant increase of average diameter from 1.8 ± 0.9 to 2.1 ± 1.0 nm.

3.2. Catalytic results

3.2.1. Effect of the ACF acidic pre-treatment on catalytic performance

It is well-known that the concentration of oxygen-containing (O-) groups on an ACF surface can be increased by acidic treatments [37]. In this study we applied a HNO_3 treatment at 298 K or 373 K to modify the ACF (see Section 2). Nickel (5 wt.%) was deposited on pre-treated and non-treated ACFs and the obtained catalysts were tested in *p*-chloronitrobenzene (*p*-CNB) to *p*-chloroaniline (*p*-CAN) hydrogenation. Fig. 7 shows that the selectivity of all the catalysts was close to 100% while the activity drastically increases (3-fold) for the ACF treated at 373 K. It is worth to noting that a yield of *p*-CAN close to 100% was obtained for all catalysts before dechlorination (cleavage C—Cl) starts. Catalytic tests also demonstrated that *in-situ* activation under H_2 of freshly prepared/passivated catalysts was necessary to obtain catalytic activity.

The effect of the ACF oxidative treatment can be related to the Ni NPs size and to the concentration and the nature of functional O-groups on the carbon surface. The HNO_3-treated carbon was previously shown to display a high density of weak and strong acid sites [44]. During the calcination step in the catalyst preparation it is likely that the strong O-containing groups (rendering CO_2 dur-

Please cite this article in press as: O. Beswick, et al., Ni-based structured catalyst for selective 3-phase hydrogenation of nitroaromatics, Catal. Today (2016), http://dx.doi.org/10.1016/j.cattod.2016.04.020

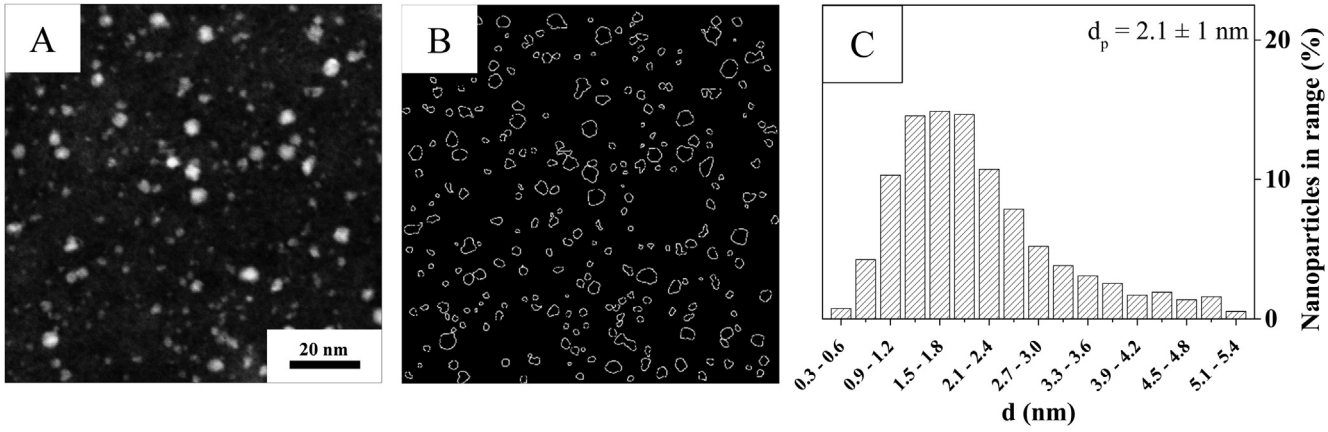

Fig. 6. Representative STEM images (A), outlines of the particles isolated after ImageJ processing (B) and related particles size distribution (C) for 5% Ni/$ACF_{HNO3-373}$ after reduction in H_2 followed by passivation.

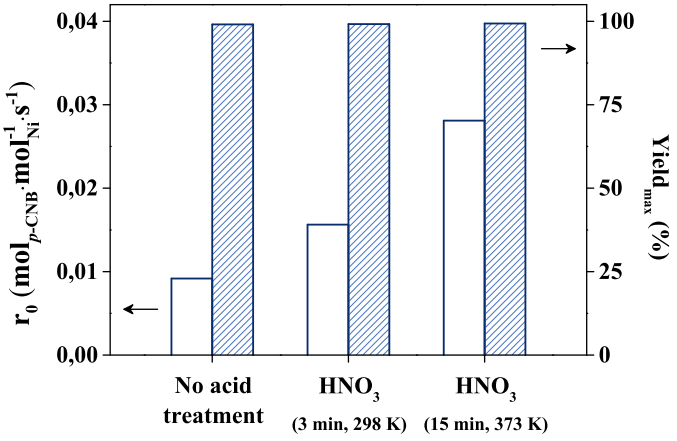

Fig. 7. Effect of ACF pre-treatment by HNO_3 on the selectivity to *p*-CAN (hatched bars) and activity (open bars) for the hydrogenation of *p*-CNB. *Reaction conditions:* T = 353 K; P_{H2} = 10 bar; $C_{p\text{-CNB},0} = 1.2 \times 10^{-1}$ mol L^{-1}, molar *p*-CNB:Ni ratio = 50.

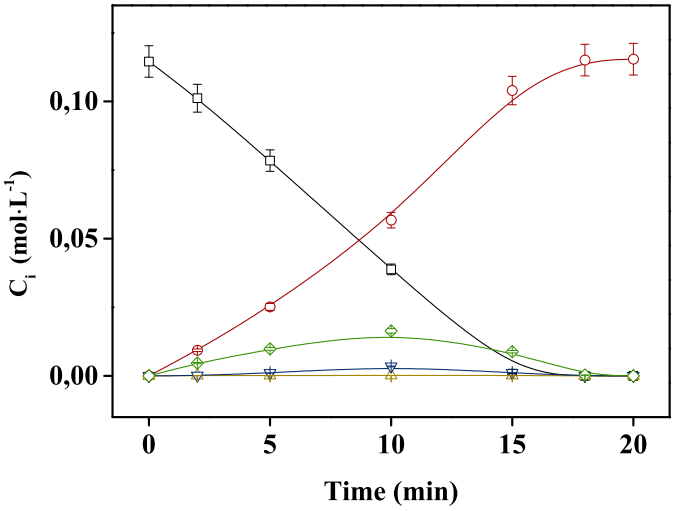

Fig. 8. Concentrations *vs* reaction time during NB hydrogenation over Ni/$ACF_{HNO3-373}$ (□ NB; ○ AN: △ azobenzene; ▽ azoxybenzene; ◇ nitrosobenzene). *Reaction conditions*: T = 353 K; P_{H2} = 10 bar; $C_{NB,0} = 1.2 \times 10^{-1}$ mol L^{-1}, molar ratio NB:Ni = 50.

ing TPD runs) were removed whereas majority of weak groups (rendering CO in TPD) remain. In fact, during TPD performed over the catalysts after the calcination step, a 60% higher amount of CO was detected from Ni/$ACF_{HNO3-373}$ as compared to Ni/ACF (4.3 *vs* 2.7 mmol g^{-1}). These weak O-groups were reported by Toebes et al. [45] to maintain the dispersion of Pt NPs on ACF while the activity towards cinnamaldehyde hydrogenation was attributed to electronic effects. Ramaker et al. demonstrated that electronegative support oxygen atoms leads to the higher ionization potential of the supported Pt NPs, increasing the TOF during hydrogenation of a tetralin ring [46]. Therefore, we suggest that the larger number of weak O-groups of Ni/ACF_{HNO3} as compared to Ni/ACF favor substrate adsorption on Ni NPs via the NO_2 group and thereby increasing the catalytic activity [47].

3.2.2. Reaction scope: nitrobenzene hydrogenation

The Ni/$ACF_{HNO3-373}$ catalyst is the most active and also has been tested in the hydrogenation of nitrobenzene (NB). Representative concentration *vs* time profiles are shown in Fig. 8. Linear dependency of NB consumption was observed until close to 100% conversion. The aniline formation passes via azo- and azoxy-intermediates indicative of the condensation route established by Haber [1]. It is important to note that the selectivity and yield of the desired aniline product continues to increase even after the full conversion of NB due to the completion of consecutive transformations of intermediates. Therefore, the maximum yield (and not the selectivity at close to full conversion) is the most important parameter to assess the catalytic performance.

The 5 wt.% Ni/$ACF_{HNO3-373}$ catalyst was also evaluated in other challenging hydrogenations (Table 2). For the nitro-aromatics containing functional groups which are sensitive to the reduction conditions (*e.g.* alkenes, halogens, *etc.*), the maximum yields of the desired anilines are the main issue. These yields were compared to ones obtained using Raney Ni under the same reaction conditions. The developed 5 wt.% Ni/$ACF_{HNO3-373}$ catalyst outperformed, by *ca.* 20-fold, the Raney Ni (industrial non-noble metal catalyst used for this reaction) in terms of activity in *p*-CNB hydrogenation and the maximum yield was also slightly higher (99.0 ± 0.5 *vs* 98.0 ± 0.5%). It is worth to note that dechlorination after reaction completion (100% conversion of *p*-CNB) was much higher over Raney Ni resulting in its rapid deactivation. At reaction completion (X = 100%), the selectivity towards aniline of 0.25% and 1.50% were obtained for the Ni/$ACF_{HNO3-373}$ and the Raney nickel catalysts, respectively. The 5 wt.% Ni/$ACF_{HNO3-373}$ catalyst was also highly efficient in *m*-dinitro-benzene hydrogenation affording a high yield of *m*-nitro-aniline (99.0 ± 0.5%).

Catalyst stability was assessed *via* 13 consecutive reaction runs using the same 5 wt.% Ni/$ACF_{HNO3-373}$ catalyst. Deactivation was more pronounced during the first run with a tendency towards

Please cite this article in press as: O. Beswick, et al., Ni-based structured catalyst for selective 3-phase hydrogenation of nitroaromatics, Catal. Today (2016), http://dx.doi.org/10.1016/j.cattod.2016.04.020

Table 2
Activity and maximum yield of the amine for the hydrogenation of nitro-aromatics (NC) over 5 wt.% Ni/ACF_{HNO3} and Raney Ni. *Reaction conditions*: T = 353 K; P_{H2} = 10 bar; $C_{NC,0} = 1.2 \times 10^{-1}$ mol L^{-1}, molar NC:Ni ratio = 50.

N°	Catalyst	Substrate (S)	Activity, $r_0 \cdot 10^2$ (mol_{NC} mol^{-1}_{Ni} s^{-1})	Maximum Yield ± 0.5 (%)	Time to reach X = 98% (min)[a]
1[b]	Ni/$ACF_{HNO3-373}$	NB	0.24	100.0	171
2		NB	3.2	100.0	15
3[b,c]		*m*-DNB	0.15	97.0	409
4		*p*-CNB	2.8	99.0	23
5	Raney Ni	*p*-CNB	0.13	98.0	672

[a] Normalized according to molar NC:Ni ratio towards the NB reduction.
[b] Without in-situ activation.
[c] Catalyst was tested at 423 K.

stabilization after the sixth run. The total activity drop (about 45%) may be due to leaching of loosely attached Ni NPs during the first run, some mechanical losses and slow accumulation of intermediates on the catalyst surface during the following reaction runs. The post-reaction mixture was analysed using AAS and no traces of Ni were detected. Therefore, the deactivation is probably due to contamination from some residuals or due to reconstructions of active sites in the course of the hydrogenation reactions, leading to the quasi-steady-state attained after 6–7 runs.

In summary, the structured 5 wt.% Ni/ACF catalyst is highly efficient for the 3-phase hydrogenation of nitro-aromatics tolerating different functionalities. In addition to obtaining near-quantitative yields of the desired anilines, the catalyst is reusable and simple to handle.

4. Conclusions

Structured catalysts consisting of small Ni NPs (~2.0 nm) supported on activated carbon fibers (ACF) have been prepared which efficiently catalyze the chemoselective hydrogenation of nitro-aromatics under relatively mild conditions (T = 353 K; P = 10 bar). The method used to prepare the catalyst was optimised, with pre-treatment of the ACF by nitric acid (prior to the impregnation by Ni-precursor) not affecting the Ni^0 dispersion, but creating a high concentration of functional O-groups leading to the enhanced (3-fold) activity of the resulting catalyst in the hydrogenation of *p*-CNB.

In-situ XRD and XPS analysis showed that the Ni NPs (generated during the calcination-reduction of the nickel salt) are metallic. The TPD and H_2-TPR data allowed the optimal reduction temperature in H_2-flow of 673 K to be established and indicated the necessity for the passivated catalyst to undergo *in-situ* activation in the reaction mixture at 353 K. Although deactivation of the catalyst was observed following storage in ambient air, catalytic activity could be regenerated by reduction at temperatures >560 K.

The best catalytic performance was observed for 5 wt.% Ni/$ACF_{HNO3-373}$, which is *ca*. 20-fold more active than the benchmark Raney Ni catalyst in the hydrogenation of *p*-CNB. Thus, the new catalyst reported here represents a significant step forward towards a simple, heterogeneous catalytic selective hydrogenation of nitroarenes that employs H_2 as the hydrogen source.

Acknowledgments

Danièle Laub and Colette Vallotton of CIME are acknowledged for the samples preparation for STEM analysis. The financial support from the Swiss National Science Foundation (Grant 200020-149869) and the Russian Science Foundation (Grant 15-19-20023) is highly appreciated.

References

[1] H.U. Blaser, H. Steiner, M. Studer, ChemCatChem 1 (2009) 210–221.
[2] R.S. Downing, P.J. Kunkeler, H. vanBekkum, Catal. Today 37 (1997) 121–136.
[3] A. Corma, P. Serna, Science 313 (2006) 332–334.
[4] A. Corma, P. Concepcion, P. Serna, Angew. Chem. Int. Ed. 46 (2007) 7266–7269.
[5] F. Cardenas-Lizana, X.D. Wang, D. Lamey, M.S. Li, M.A. Keane, L. Kiwi-Minsker, Chem. Eng. J. 255 (2014) 695–704.
[6] F. Cardenas-Lizana, D. Lamey, N. Perret, S. Gomez-Quero, L. Kiwi-Minsker, M.A. Keane, Catal. Commun. 21 (2012) 46–51.
[7] F. Cardenas-Lizana, S. Gomez-Quero, M.A. Keane, ChemSusChem 1 (2008) 215–221.
[8] F. Cardenas-Lizana, S. Gomez-Quero, M.A. Keane, Catal. Commun. 9 (2008) 475–481.
[9] A. Corma, P. Serna, P. Concepcion, J.J. Calvino, J. Am. Chem. Soc. 130 (2008) 8748–8753.
[10] E. Joannet, C. Horny, L. Kiwi-Minsker, A. Renken, Chem. Eng. Sci. 57 (2002) 3453–3460.
[11] R. Raja, V.B. Golovko, J.M. Thomas, A. Berenguer-Murcia, W.Z. Zhou, S.H. Xie, B.F.G. Johnson, Chem. Commun. (2005) 2026–2028.
[12] F. Cardenas-Lizana, C. Berguerand, I. Yuranov, L. Kiwi-Minsker, J. Catal. 301 (2013) 103–111.
[13] B. Coq, A. Tijani, F. Figueras, J. Mol. Catal. 68 (1991) 331–345.
[14] V. Holler, D. Wegricht, I. Yuranov, L. Kiwi-Minsker, A. Renken, Chem. Eng. Technol. 23 (2000) 251–255.
[15] R.V. Jagadeesh, A.E. Surkus, H. Junge, M.M. Pohl, J. Radnik, J. Rabeah, H.M. Huan, V. Schunemann, A. Bruckner, M. Beller, Science 342 (2013) 1073–1076.
[16] F.A. Westerhaus, R.V. Jagadeesh, G. Wienhofer, M.M. Pohl, J. Radnik, A.E. Surkus, J. Rabeah, K. Junge, H. Junge, M. Nielsen, A. Bruckner, M. Beller, Nat. Chem. 5 (2013) 537–543.
[17] K. Bhaumik, K. Akamanchi, Can. J. Chem. 81 (2003) 197–198.
[18] F. Cardenas-Lizana, S. Gomez-Quero, M.A. Keane, Appl. Catal. A Gen. 334 (2008) 199–206.
[19] M.V. Twigg, M.S. Spencer, Appl. Catal. A Gen. 212 (2001) 161–174.
[20] L.Z. Nikoshvili, A.S. Makarova, N.A. Lyubimova, A.V. Bykov, A.I. Sidorov, I.Y. Tyamina, V.G. Matveeva, E.M. Sulman, Catal. Today 256 (2015) 231–240.
[21] G.C. Bond, Chem. Soc. Rev. 20 (1991) 441–475.
[22] N. Semagina, L. Kiwi-Minsker, Catal. Rev. 51 (2009) 147–217.
[23] A. Borodzinski, Catal. Lett. 71 (2001) 169–175.
[24] N. Semagina, L. Kiwi-Minsker, Catal. Lett. 127 (2009) 334–338.
[25] M. Crespo-Quesada, A. Yarulin, M.S. Jin, Y.N. Xia, L. Kiwi-Minsker, J. Am. Chem. Soc. 133 (2011) 12787–12794.
[26] L. Kiwi-Minsker, I. Yuranov, V. Holler, A. Renken, Chem. Eng. Sci. 54 (1999) 4785–4790.
[27] S.R. de Miguel, J.I. Villella, E.L. Jablonski, O.A. Scelza, C.S.M. de Lecea, A. Linares-Solano, Appl. Catal. A Gen. 232 (2002) 237–246.
[28] M.C.M. Perez, C.S.M. deLecea, A.L. Solano, Appl. Catal. A Gen. 151 (1997) 461–475.
[29] V. Gaur, A. Sharma, N. Verma, Carbon 43 (2005) 3041–3053.
[30] J. Economy, M. Daley, C. Mangun, Abstr. Pap. Am. Chem. Soc. 211 (1996) 84 (Fuel).
[31] C. Wang, J.S. Qiu, C.H. Liang, L. Xing, X.M. Yang, Catal. Commun. 9 (2008) 1749–1753.
[32] N. Mahata, A.F. Cunha, J.J.M. Orfao, J.L. Figueiredo, Appl. Catal. A Gen. 351 (2008) 204–209.
[33] N. Mahata, A.F. Cunha, J.J.M. Orfao, J.L. Figueiredo, Catal. Commun. 10 (2009) 1203–1206.
[34] V. Holler, D. Wegricht, I. Yuranov, L. Kiwi-Minsker, Chem. Eng. Sci. Technol. 23 (2000) 251–255.
[35] D. Rosenthal, M. Ruta, R. Schlogl, L. Kiwi-Minsker, Carbon 48 (2010) 1835–1843.
[36] C. Subrahmanyam, D.A. Bulushev, L. Kiwi-Minsker, Appl. Catal. B Environ. 61 (2005) 98–106.
[37] J.L. Figueiredo, M.F.R. Pereira, M.M.A. Freitas, J.J.M. Orfao, Carbon 37 (1999) 1379–1389.
[38] S. Brunauer, P.H. Emmett, E. Teller, J. Am. Chem. Soc. 60 (1938) 309–319.
[39] J.W. Shim, S.J. Park, S.K. Ryu, Carbon 39 (2001) 1635–1642.
[40] G.B. Baur, I. Yuranov, L. Kiwi-Minsker, Catal. Today 249 (2015) 252–258.
[41] W. Brockner, C. Ehrhardt, M. Gjikaj, Thermochim. Acta 456 (2007) 64–68.
[42] H.S. Johnston, L. Foering, Y.S. Tao, G.H. Messerly, J. Am. Chem. Soc. 73 (1951) 2319–2321.
[43] M.C. Biesinger, B.P. Payne, L.W.M. Lau, A. Gerson, R.S.C. Smart, Surf. Interface Anal. 41 (2009) 324–332.

Please cite this article in press as: O. Beswick, et al., Ni-based structured catalyst for selective 3-phase hydrogenation of nitroaromatics, Catal. Today (2016), http://dx.doi.org/10.1016/j.cattod.2016.04.020

[44] G.C. Torres, E.L. Jablonski, G.T. Baronetti, A.A. Castro, S.R. deMiguel, O.A. Scelza, M.D. Blanco, M.A.P. Jimenez, J.L.G. Fierro, Appl. Catal. A Gen. 161 (1997) 213–226.
[45] M.L. Toebes, Y.H. Zhang, J. Hajek, T.A. Nijhuis, J.H. Bitter, A.J. van Dillen, D.Y. Murzin, D.C. Koningsberger, K.P. de Jong, J. Catal. 226 (2004) 215–225.
[46] D.E. Ramaker, J. de Graaf, J.A.R. van Veen, D.C. Koningsberger, J. Catal. 203 (2001) 7–17.
[47] B. Coq, A. Tijani, R. Dutartre, F. Figueras, J. Mol. Catal. 79 (1993) 253–264.

Please cite this article in press as: O. Beswick, et al., Ni-based structured catalyst for selective 3-phase hydrogenation of nitroaromatics, Catal. Today (2016), http://dx.doi.org/10.1016/j.cattod.2016.04.020